Bifurcation and chaos in a system of Taylor vortices: a natural and numeriacal experiment

V. S. L'vov, A. A. Prdetechenskiĭ, and A. I. Chernykh

Institute of Automation and Electrometry, Siberian Division of the Academy of Sciences of the USSR

The appearance of turbulence in cylindrical Couette flow is experimentally and theoretically investigated. The loss of the stability of the Taylor vortices leads to the appearance of strictly periodic oscillations in the flow. It is shown that as the Reynolds number increases these oscillations acquire, as a result of the destruction of the spatial coherence, a deep slow modulation that subsequently becomes chaotic. A system of ordinary differential equations describing the dynamics of the interacting vortices at this stage is proposed. The behavior of the model in a numerical experiment qualitatively corresponds to the change of flow regimes observed in a natural experiment.

INTRODUCTION

It can now be considered to be generally acknowledged that the transition from laminar flow of a liquid to turbulent flow can be described with the aid of a finite system of ordinary differential equations. This system is usually obtained by reducing the Navier–Stokes equations by the method of approximating functions (i.e., by Galerkin's method). In such an approach, the onset of turbulence is related[1,2] to the formation of a stochastic attractor in the phase space of this multidimensional dynamical system. Normally, the stochastic attractor[3] is a closed attracting set of trajectories, which, however, disperse everywhere exponentially, so that a trajectory taken separately is forced to behave highly intricately—in the strict sense, chaotically. But the study of the question of the relationship between the stochastic attractors and the onset of turbulence is only beginning.

The first steps in this direction have been taken in the study of extremely simple convection flows. It is shown in Ref. 4 that the initial stage of the development of stochasticity in a convection loop is described by the well-known Lorenz system of three differential equations.[5] Sinai[3] and Lyubimov *et al.*[6] have used for the description of thermoconvection in a plane layer (i.e, in a Haley–Shaw cell) eight equations that reveal stochastic behavior in a numerical simulation. The number of usable equations increases sharply when we attempt to describe more complex flows.[7,8] This is due to the fact that an almost arbitrarily chosen basis of approximating functions is usually quite different from the eigenbasis even for the simplest regimes that arise not far beyond the instability threshold. This leads to an unwarrantably large number of equations, and makes the analysis of their solutions extremely difficult. But the truncation of the formal Galerkin·series can lead to a change in the subtle characteristics of the attractor structure of the initial multidimensional system: the stochastic attractor may be converted into a complex limit cycle. Further truncation of the system may convert the cycle into another stochastic attractor, so that it remains unclear whether the attractors constructed in this way bear a direct relation to the problem of the development of turbulence. Therefore, the first question that arises is this: How many, and precisely which, equations are necessary for a reasonably accurate description of specific flows at different Reynolds numbers?

It may be pointed out here that in a number of problems with Reynolds numbers characterizing the transition from the laminar regime to the developed-turbulence regime the main energy of the liquid is concentrated in narrow frequency regions of the power spectrum. Therefore, the velocity $v(r,t)$ can be represented in the form

$$v(r, t) = \mathrm{Re}\left[\sum_j A_j(r, t) \exp(i\omega_j t) \right], \qquad (1)$$

where, in contrast to $v(r,t)$, the "complex mode envelopes" $A_j(r,t)$ are slowly varying functions of the time with characteristic time scales of the order of the inverse line width $\Delta\omega_j^{-1}$. We can, in some small domain of variation of the Reynolds number, neglect the variation of the spatial structure of the "fast" ω_j modes, and, assuming that $A_j(r, t) = A_j(t) f_j(r)$, write down phenomenological equations for $A_j(t)$, retaining in them only the resonance terms, and taking no interest in the specific spatial structure of $f_j(r)$. We can call the quantities $A_j(t)$ thus constructed effective phase variables, and formulate in such terms a number of questions for experiment: What is the dimensionality of the effective phase space of the given hydrodynamic flow in the specific narrow range of Reynolds numbers? What is the character of the phase trajectory as $t \to \infty$, i.e., what is the structure of the attractor? How does it vary with increasing Reynolds number? And, finally, what is the relationship between the experimentally observed attractor structure and the structure that arises in a numerical modeling of the phenomenological equations?

In the present paper we study these questions in the particular case of the transition to turbulence in circular Couette flow. The hydrodynamic unit of the setup[9] (see also the Appendix) consisted of a stationary cylindrical container of diameter $d_2 = 55$ mm and height $h = 305$ mm, in which a rod of diameter $d_1 = 35$ mm rotated. The azimuthal velocity component v_φ was measured with a laser Doppler velocimeter (LDVM) at a fixed point whose vertical coordinate could be varied

within the limits from 80 to 120 mm from the top of the cylinders, while the radial coordinate was chosen to be that of the middle of the gap. To begin with, we shall in §1 briefly describe the process of Taylor–vortex formation, and discuss the evolution of the power spectrum in a broad range of Reynolds numbers (from 10^2 to 10^4) in order to obtain information about the order of appearance, and the number of, the "fast" motions. In §2 we present more detailed experimental data in the range of Reynolds numbers from 1000 to 1200, in which the coherence of the flexural vibrations is destroyed and the flow of the liquid becomes stochastic. Further, in §3 we propose a phenomenological system of equations, (3.4), for the flexure amplitudes in the Taylor-vortex pairs, and study the analytically simplest steady states of the system and their stability. In §4 we present preliminary results of a numerical simulation of this system. This simulation reveals a wide variety of attractors, including quite complex ones, and the sequence of bifurcations for some values of the parameters coincides with the experimentally observed sequence. In §5 we carry out a numerical investigation of the simplest statistical properties of the trajectories on a complex attractor, and estimate its dimensionality.

§1. PRELIMINARY EXPERIMENTS

1. Appearance of Taylor vortices

As is well known,[10] there should form in almost any real circular Couette flow, as the Reynolds number adiabatically increases, a strictly fixed "optimal" number, $\tilde{N}_0$, of Taylor vortices. This state is created not through bifurcation, but smoothly from the state with $Re = 0$, although the amplitude of this motion becomes appreciable only upon the attainment of a Reynolds number close to the critical Reynolds number (Re_c) of an idealized infinitely long system, and subsequently varies according to the square root law [$\sim (Re - Re_c)^{1/2}$] for normal bifurcation.

In our setup the Taylor vortices first become observable at $Re = 74 \pm 2$. We determine the Reynolds number from the expression $Re = \omega_m d_1(d_2 - d_1)/4\nu$, where ω_m is the angular velocity of the inner cylinder and ν is the coefficient of kinematic viscosity. To obtain an optimal unique state, we employed the following procedure: at $Re = 65$ (which for water corresponds to a rotation period $T \approx 20$ sec at $t = 24\,°C$) we waited for one hour and then increased the Reynolds number according to a linear law to 85 over a period of 5 hours. In the process, in nine out of ten cases the state with $N_0 = 30$ was created. Other stable steady states with 22 to 36 vortices could be realized in the setup with rougher acceleration regimes.[9]

2. Evolution of the power spectrum

As the Re is increased, the secondary steady states with different $\tilde{N}$ in our setup remain stable right up to high supercriticalities: $Re \approx (6-13)Re_c$, so that up to this moment the measured quantity $v_\varphi(t) = const$. Further increase of the Re leads to the excitation of nonstationary flow regimes. The series of power spectra $J(\omega)$ measured for a number of successively increasing
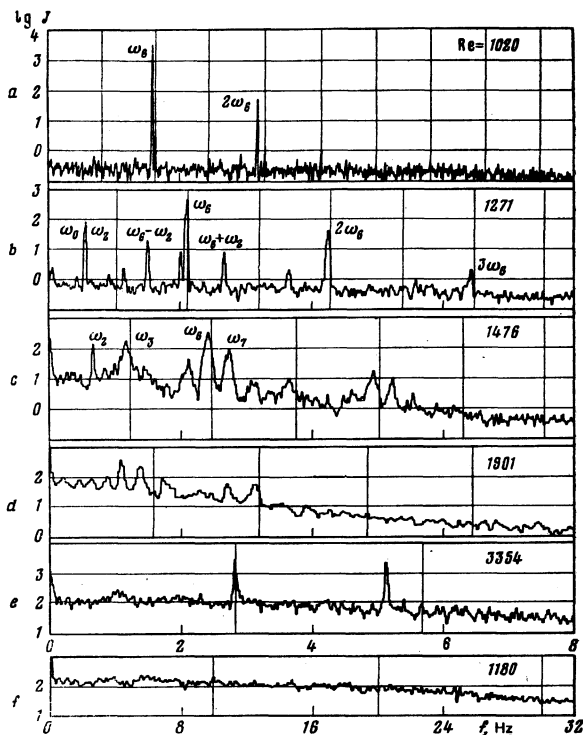

FIG. 1. Evolution of the velocity power spectrum $J(\omega)$ for flow with 30 Taylor vortices. The vertical lines indicate the harmonics of the rotation frequency of the inner cylinder; the numbers, the frequency in Hertz. The use of the "Henning window" gives a 3/512 frequency resolution for the entire scale.

Re values shows that the representation (1) is indeed valid at the initial stage of the turbulization. The power spectrum was computed according to the expression

$$J(\omega) = \langle |v_\omega|^2 \rangle, \qquad (1.1)$$

where v_ω is the Fourier transform of $v_\varphi(t)$ and $\langle \ldots \rangle$ denotes averaging over the successive segments of the $v_\varphi(t)$ realization. The detailed evolution of the spectrum for flows with $\tilde{N}$ equal to 28, 29, and 30 is discussed in Ref. 11. Here we restrict ourselves to the description of the evolution of the $\tilde{N}_0 = 30$ optimal state (Fig. 1). We can follow the succession of bifurcations leading to the excitation of new modes of motion. Thus, at $Re \approx 1000$ there are excited flexural vibrations of the vortices (6 bends along the circumference of a vortex), and a sharp peak appears in the power spectrum at the frequency $\omega_6 = 1.93\omega_m$. The relative width of this peak is equal to 10^{-3} at a level of 10^{-3} from the maximum.

In the $Re \approx 1040-1140$ region we observed a number of bifurcations leading to the appearance of a fine structure in the ω_6 line and a slight broadening of the line ($\Delta\omega_6/\omega_6 \approx 10^{-2}$ at $Re = 1040$). A low-frequency motion with characteristic times $\Delta\omega_6^{-1}$ then arises. Later, in the range $Re \approx 1200 - 1300$, there arise successively motions at the incommensurable frequencies $\omega_2 = 0.55\omega_m$ and $\omega_3 = 0.95\omega_m$ and their combination harmonics. Subsequently, the widths of the peaks gradually become comparable to their spacing. The spectrum no longer contains well pronounced peaks at $Re \approx 1900$. Upon further increase of Re, sharp peaks appear in the

TABLE I. Bifurcation parameter values for the first reconstructions of Couette flow.

	Data of Refs.		
	11		13
Cylinder height/gap	30		20
Ratio of gap to radius of inner cylinder	0.57		0.14
Appearance of Taylor vortices	$Re_c = 74 \pm 2$		$Re_c = 120$
Number of Taylor vortices	30	28	17
Appearance of azimuthal waves	$Re/Re_c = 13$	$Re/Re_c = 6.5$	$Re/Re_c = 1.3$
Number of generated flexures	6	1	4
Stability region for the azimuthal waves $(Re - Re_1)/Re_1$	0.025	0.8	14

FIG. 2. Fine structure of the ω_6-peak evolution. The vertical line indicates the frequency $2\omega_m$.

continuous-spectrum background. Then this system of secondary peaks are destroyed in the same way as the primary system. At very high Re (the bottom figure) the spectrum turns out to be continuous, but even in this case remnants of the steady-state spatial structure can be observed, although in the temporal aspect the flow has already been highly turbulized.

It should be noted that the way to turbulence in Coutte-Taylor flow (the sequence of bifurcation Reynolds numbers, the type of motions arising then, the character of the peak broadening in the power spectrum, etc.) depends not only on the geometric dimensions of the cylinders and the boundary conditions at the ends, but also on the number of vortices that arise in the same setup (Table I). But the rough, qualitative aspects of the pattern of transition to turbulence are on the whole general.[11] Among them is, for example, the fact that, as the Re increases, bifurcations occur which lead to the appearance of sharp peaks in the spectrum, to the broadening of the spectral peaks appearing earlier, as well as to the appearance of peaks of finite width. Also fairly general is the presence, strongly manifested in Couette flow, of several metastable flows in the intermediate range of Re numbers. All this points to the fact that a Couette flow with a rotating internal cylinder is a convenient model for the study of a number of general qualitative characteristics of a smooth, somewhat phased regime of transition to turbulence.

§2. DESTRUCTION OF THE COHERENCE OF THE FLEXURAL VIBRATIONS

As has already been noted, at Re > 1040, the ω_6 line of the power spectrum broadens. We shall show that this phenomenon has a fundamentally important character, and indicates a transition to stochastic (unpredictable at large times) flow. In our setup, these processes have quite a slow character, and we investigated them using the following procedure. After the process of growing the optimal Taylor vortices, the Re number was smoothly increased at a rate of ~200/h to the supercritical value Re $\approx 1050 - 1100$. After 10–20 minutes vibrations with frequency $\omega_6 \approx 1.6$ Hz were excited in the flow. Then the measuring volume was moved along the z axis to the place where the signal was strongest (see Ref. 11), and the Re number was decreased in small steps ($\Delta Re \approx 20$/h) until the state with $A(t) = $ const was attained. Then we decreased the Re in even smaller steps ($\Delta Re \approx 5-10$), and at each step
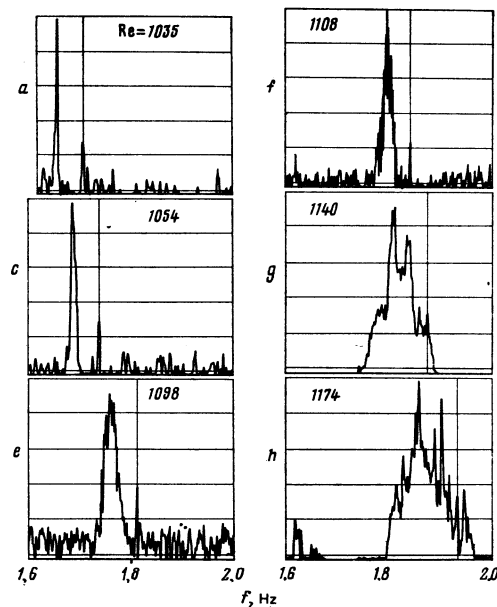
waited for the establishment of the steady-state amplitude (0.5–2 hours, depending on the supercriticality), after which the observable signal was recorded with the aid of a system for the collection and display of data.[12] A typical realization length for the estimation of the amplitude was 1024 sec, with 16 counts in a second (8192 counts), while for the analysis of the character of the signal this length reached 256 thousand counts.

After getting fairly close to the threshold from above, we again increased the Re number in steps, and, after waiting at each step till the transient processes were over (1–1.5 h), made a record of the realization. The application to these realizations of the traditional techniques of spectral analysis with high frequency resolution yields the result shown in Fig. 2, from which it can be seen that, above Re ≈ 1100, the spectral line acquires a complex fine structure as a result of the deviation of the observed signal from monoharmonic. A much greater amount of information about the flow can be obtained by using the envelope representation (1), and
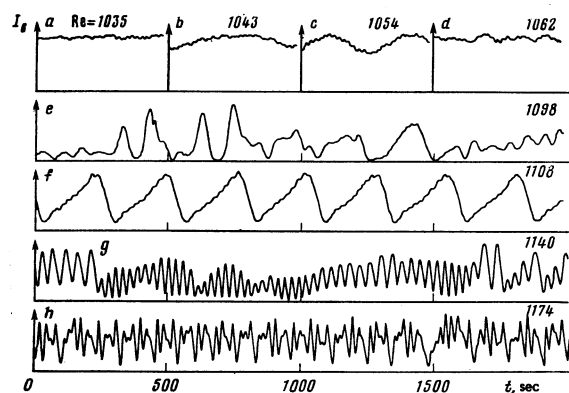

FIG. 3. Time dependences of the ω_6-peak intensity (in the $(1 \pm 0.02)\omega_6$ frequency window. A 2000-sec time interval corresponds to ~ 3500 periods of the fundamental motion.

computing the time dependence of the amplitude of the ω_6 peak with the aid of one of the narrow-band digital filtration algorithms. We employed a filter with a Gaussian window and a width equal to the peak width at the 10^{-3} level. These results are shown in Fig. 3. In the first regime (Figs. 2a and 3a with Re = 1035), with a supercriticality Re $-$ Re$_1 = 2 \times 10^{-2}$Re$_1$, the amplitude $A_6(t)$ does not vary in time, which corresponds to a periodic motion with frequency ω_6, whose image in the phase space of the fast variables is a stable limit cycle. In this case the characteristic vibration amplitudes measured in neighboring vortices differ by not more than 10%.

The next two regimes [the regimes b) and c) in Fig. 3, as well as the regime c) in Fig. 2] correspond to Re numbers, 1043 and 1054, exceeding some bifurcation value, Re$_1^{(1)}$, that gives rise to a slow sinusoidal modulation of the fundamental motion, whose frequency, ω_0, increases with increasing supercriticality. This modulation, which is clearly visible in Figs. 3b and 3c, is not manifested in the spectra because of the finiteness of the resolution.[1] The image of the motion depicted here is a simple attractor—a two-dimensional torus. It is, of course, possible that the modulation in Figs. 3b and 3c is not strictly periodic.

Further increase of the Reynolds number leads to the occurrence of a series of closely positioned bifurcations whose observation is made difficult by the extreme slowness of the steady-state establishment process. Therefore, we cannot be entirely certain that the regimes described below directly replace each other as the Re is increased. Thus, the periodic modulation described below does not occur when Re = 1062, a simple limit cycle being observed (Fig. 3d). At Re = 1098 we observe a complex modulation that can be described as chaotic, as far as we can judge from observations made over a relatively short period of time. The ω_6 peak for this Re number (Fig. 2e) turns out to be appreciably broadened. The fact that with increasing Reynolds number the modulation again becomes periodic, although not sinusoidal, but saw-toothed (Figs. 2f and 3f for Re = 1108), is extremely interesting. Subsequently (Figs. 2g and 3g, Re = 1140), the nature of the modulation again becomes complex. With a certain imagination, we can see in Fig. 3g alternating segments of sinusoids of different frequencies. Accordingly, the ω_6 peak in Fig. 2g is split into two broad peaks. Let us also note that the modulation frequency in this regime is an order of magnitude higher than in the preceding regime. At Re = 1174 (Fig. 2h), the spectral line exhibits on its right slope a narrow peak with two satellites, a fact which indicates the presence in the amplitude modulation of a periodic component not present in the preceding regime.

In the last regimes we can, by moving the measuring volume of the LDVM along the z axis, observe that the vortices vibrate in pairs: in each interval of time the amplitude of the ninth vortex is equal to the amplitude of the tenth vortex, while the eleventh and twelfth have the same aplitude. However, the amplitudes of these vortex pairs can differ by a factor of two to three,
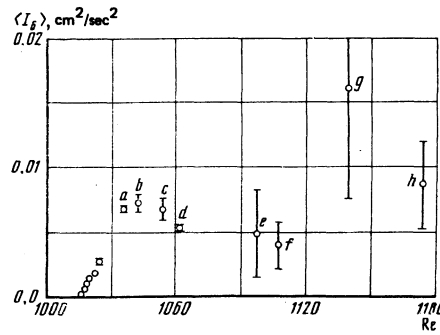

FIG. 4. The ω_6 peak's mean amplitude and its variance (whiskers) as a function of the Reynolds number. The letters a-h correspond to the regimes depicted in Figs. 2 and 3.

and this relation and its sign vary in time in a complicated fashion. From this it can be inferred that the destruction of the limit cycle in our setup is due first and foremost to the destruction of the spatial coherence of the flow, and not to internal processes in the vortex pair. Only when the Re is increased further does a new "fast" motion—the ω_2 mode—arise.

The computation of the mean value and the variance of the square of the slow amplitude yields the result shown in Fig. 4, from which it can be seen that the $\langle |A|^2 \rangle$ values for small supercriticalities lie on the straight line $\langle |A|^2 \rangle \sim$ Re $-$ Re$_1$. This allows us to estimate Re$_1$ to within ± 1 in each experiment. In our experiments we found three Re$_1$ values: 995, 1005, and 1015. If, after the creation of some state with a definite Re$_1$, the system is not taken far and for a long time into the subcritical region, then this state exists for an indefinitely long period of time. For example, there are among the data shown in Fig. 4 on the initial segment of the dependence points that were obtained two days after the beginning of the experiment, and they lie on the same curve (for greater details, see Fig. 3.3 in Ref. 11). But if we return to the subcritical region, wait there for the vibrations to be completely damped out, and then let the system again rise abruptly above the instability threshold, then $\langle |A|^2 \rangle$ as a single valued function of Re cannot be reproduced. The causes of this are as yet unclear. Nevertheless, these states subsequently evolve in a qualitatively similar fashion: we first observe a long-wave modulation, which subsequently disappears in a narrow range of Re values, after which there arises a complex modulation that subsequently develops into a higher-frequency modulation.

§3. PHENOMENOLOGICAL MODEL FOR A SYSTEM OF INTERACTING TAYLOR VORTICES

1. The basic equations

The spectrum for small supercriticalities above the threshold Re$_1$ contains peaks at the frequencies ω_6 and $2\omega_6$. We can accordingly write down a system of equations for the envelopes A and B of these motions, retaining only the resonance terms in it:

$$dA/dt = \gamma A + v_1 B A^* + w|A|^2 A, \quad dB/dt = -\tilde{\gamma} B + v_2 A^2. \quad (3.1)$$

For Re = Re$_1$, $\gamma = 0$, and it is therefore natural to set

$\gamma = \alpha(\text{Re} - \text{Re}_1)$. For small supercriticalities $\gamma \gg \tilde{\gamma}$, and therefore the characteristic time, τ, for the motion should be longer than $\tilde{\gamma}^{-1}$. This means that we shall be able to neglect d/dt as compared to $\tilde{\gamma}$ in the equation for B. In that case the B motion will become a forced motion:

$$B = v_2 A^2 / \tilde{\gamma}. \tag{3.2}$$

These arguments can be justified experimentally. In the first place, it follows from (3.2) that the phases (ψ_1 and ψ_2) of the A and B motions should be rigidly correlated: $2\psi_1 - \psi_2 = \text{const}$, so that the quantity $|\Phi|$, where

$$\Phi = \langle v(\omega_6) v^*(2\omega_6) / |v(\omega_6)v(2\omega_6)| \rangle,$$

should be equal to unity. Its computation from the experimental data yields the value 0.98–0.99 right up to Re = 1300.

Further, the quantities $I_A(t) = |A(t)|^2 = I_6$ and $I_B(t) = |B(t)|^2$, as computed from the experimental data on the velocity $v(t)$, can be regarded as a parametric representation in the $X-Y$ plane of the projection of the phase trajectory. Since this trajectory contains a random component, it is natural to construct the probability density for the system to stay at one point of the phase plane, and analyze only the regression lines: $\langle X \rangle$ as a function of Y and $\langle Y \rangle$ as a function of X. The results of such a analysis show that the regression lines are concentrated along the parabola corresponding to the consequence of the relation (3.2): $B(t) \sim A^2(t)$. By taking the square root of the Y coordinate, we straighten the parabola, and obtain a straight line. It follows from all this that the motion at the frequency $2\omega_6$ is a forced motion, and is therefore not an effective degree of freedom, so that, with allowance for (3.2), the system (3.1) reduces to the standard form:

$$dA/dt = \gamma A + (iT - \eta)|A|^2 A, \quad \gamma = \alpha(\text{Re} - \text{Re}_1). \tag{3.3}$$

This equation has a unique solution which expresses the Landau law: $|A|^2 = \gamma/\eta = \alpha(\text{Re} - \text{Re}_1)/\eta$. Figure 4 shows that it is well fulfilled in experiment in the region $\text{Re}_1 < \text{Re} < \text{Re}_1^{(1)}$, where a stable limit cycle exists. But this equation does not explain the destruction of the limit cycle, i.e., the appearance of the time dependence $A(t)$. The point is that, in deriving it, we assumed the absence of any degeneracy, assuming that the ω_6 flow is described by the unique spatial function $f_6(r)$: $A(t)f_6(r)$. At the same time, the visualization of the flow shows that, even in the case of an appreciable flexure amplitude, the boundary between pairs of vortices almost does not vibrate. Consequently, the first approximation, the flow in each pair is independent, and the flexure amplitude of the n-th vortex pair has its own equation (3.3) to be written down [see the first line in (3.4)]. Thus, the ω_6 flow has a high degeneracy multiplicity (equal to the number of vortex pairs $N = \tilde{N}/2$), which is due to the great relative height of the cylinder: $h \gg r_2 - r_1$. On account of the weakness, noted above, of the interaction between neighboring pairs, we shall take this interaction into consideration only in the linear approximation:

$$dA_n/dt = \gamma A_n + (iT - \eta)|A_n|^2 A_n$$
$$+ \tfrac{1}{4}(a + ib)(A_{n+1} + A_{n-1} - 2A_n), \quad n = 1, \dots, N. \tag{3.4}$$

We must assume that $\gamma > 0$ and $\eta > 0$ in this equation, and we can, without loss of generality, assume that $a > 0$. It is reasonable to assume that only γ depends on the Re number.

2. The steady-state solutions in an unbounded cylinder and their stability

The number of vortex pairs in our setup is fairly high: $N = 15$. It is therefore reasonable to initially assume in an analytical investigation of equations of the type (3.4) that $N \gg 1$, and neglect the boundary conditions. It is then clear that for $\gamma > 0$ this equation has a non trivial, spatially homogeneous solution that coincides with the solution to Eq. (3.3):

$$A_n(t) = A^0(t) = A^0 \exp(i\gamma Tt/\eta), \quad |A^0|^2 = \gamma/\eta. \tag{3.5}$$

Let us investigate the stability properties of this solution. For this purpose, let us assume that A_n differs from A^0 by a small quantity δA_n, and linearize Eqs. (3.4) with respect to δA_n, which we represent in the form:

$$\delta A_n = \varepsilon A^0 \exp(\nu t + 2i\psi n). \tag{3.6}$$

Then the system of linearized equations for δA_n reduces to a pair of complex equations for ε and ε^*, the condition for the vanishing of whose determinant yields an expression for the increment of the "modulation instability:"

$$\nu_\psi = -(\gamma + a_\psi) \pm [\gamma^2 - b_\psi(b_\psi - 2\gamma T/\eta)]^{1/2}, \tag{3.7}$$
$$a_\psi = a \sin^2 \psi, \quad b_\psi = b \sin^2 \psi.$$

It can be seen that $\nu_0 = 0$; for small ψ

$$\nu_\psi = (bT - a\eta) \sin^2 \psi / \eta. \tag{3.8}$$

Thus, $\nu_\psi > 0$ when $bT > a\eta$, and the spatially homogeneous solution (3.5) is unstable against the amplitude modulations (3.6). The boundary, ψ_0, of the instability region can be found from (3.7) after setting $\nu_{\psi_0} = 0$:

$$\sin^2 \psi_0 = 2\gamma(bT - a\eta)/\eta(a^2 + b^2). \tag{3.9}$$

It also follows from (3.7)–(3.9) that, in the opposite case, i.e., when $a\eta > bT$, $\text{Re}\,\nu_\psi < 0$ for any ψ, and the solution (3.5) is stable.

3. The steady-state solutions in a bounded cylinder

In a bounded cylinder, it is necessary to allow for the fact that the equations for the extreme vortex pairs (with $n = 1$ and $n = N$) differ from (3.4), for each of them interacts not with two but with only one vortex pair (with $n = 2$ and $n = N - 1$, respectively). Formally, this circumstance can be taken into consideration by imposing the following "boundary conditions" on the admissible solutions to Eqs. (3.4):

$$A_0 = A_{N+1} = 0. \tag{3.10}$$

For small supercriticalities it is convenient to seek the solutions to (3.4) in the form of an expansion in terms of the harmonics B_m:

$$A_n = \sum_{m=1}^{N} B_m \sin[\pi mn/(N+1)],$$

$$(N+1)B_m = 2 \sum_{n=1}^{N} A_n \sin[\pi mn/(N+1)], \tag{3.11}$$

which automatically satisfy the condition (3.10). This representation is also convenient in that it diagonalizes the linear part of Eqs. (3.4):

$$dB_n/dt = -(\gamma_n + ib_n)B_n + (NL)_n. \tag{3.12}$$

Here we have introduced the notation

$$\gamma_n = (-\gamma + a_n), \quad a_n = a\sin^2[\pi n/2(N+1)],$$
$$b_n = b\sin^2[\pi n/2(N+1)]. \tag{3.13}$$

The nonlinear part of (3.12) appears to be quite complicated:

$$(NL)_n = \frac{iD}{2}\sum_{n_1,n_2,n_3=-N}^{N} B_1 \cdot B_2 B_3$$

$$\times[\Delta(n+n_1+n_2+n_3)+\Delta(n+n_1+n_2+n_3+2N+2)$$
$$+\Delta(n+n_1+n_2+n_3-2N-2)], \quad D=8(T+i\eta)/(N+1), \tag{3.14}$$

where $B_i = B_{n_i}$, B_{-n}, and Δ is the Kronecker symbol: $\Delta(0)=0$ and $\Delta(n)=1$ for $n\neq 0$.

Equation (3.12) allows us to find easily the instability threshold for the zeroth-order solution with respect to the excitation of the n-th harmonic: $\gamma_n = 0$. The first to be excited is the harmonic B_1 when

$$\gamma > a_1 = a\sin^2(\pi/2(N+1)). \tag{3.15}$$

As was to be expected, as the length of the cylinder is increased (i.e., as $N \to \infty$), the excitation threshold for the first harmonic tends to the threshold for the appearance of the spatially homogeneous solution (3.5), $\gamma = 0$.

It follows from the structure of Eqs. (3.12)–(3.14) that three types of solutions can occur: a) with vanishing even harmonics, b) with vanishing odd harmonics, and c) a solution of the general form; the last solution is twofold degenerate—with respect to a change of sign of the even harmonics. In this case

$$B_1(t) = |B_1|\exp i\delta_1 t, \quad |B_1|^2 = |\gamma_1|(N+1)/12\eta,$$
$$\delta_1 = -(b_1 + \gamma_1 T/\eta), \quad B_3(t) = |B_3|\exp i\delta_1 t, \tag{3.16}$$
$$|B_3|^2 = |B_1|^2\gamma_1^2(T^2+\eta^2)/9\eta^2[\gamma_3^2+(b_1^2-b_3^2)].$$

This solution has been obtained from (3.12)–(3.14) under the assumption that $|B_3| \ll |B_1|$, i.e., for small supercriticalities. It can be shown that it is stable in this region against the excitation of the even harmonics.

Let us now show that, as the supercriticality increases, the solution to Eqs. (3.4) with the null "boundary conditions" (3.10) tends to the spatially homogeneous solution (3.5) in the case in which it is stable, i.e., when $a\eta > bT$.

Let us first investigate the approach of (3.5) to its asymptotic form as the distance from the boundary increases, i.e., as n increases. For this purpose, we assume that $A_n(t)$ differs from A^0 by a small quantity δA_n, and linearize (3.4) with respect to δA_n, which we represent in the form

$$\delta A_n = \varepsilon A^0(t)\exp(-2\varkappa n). \tag{3.17}$$

Then we obtain for ε and ε^* a pair of complex equations, the condition for the vanishing of whose determinant yields

$$C = \mathrm{sh}^2\varkappa = 2\gamma(a\eta - bT)/\eta(a^2+b^2). \tag{3.18}$$

The solution to this equation has the form

$$\exp(2|\varkappa|) = 2C+1+2(C^2+C)^{1/2}. \tag{3.19}$$

From this it can, for example, be seen that even with $C=\frac{1}{2}$ the difference δA_n decreases very rapidly with increasing n: $\delta A_{n+1}/\delta A_n \approx 0.21$. All this is a manifestation of the symmetry of the initial problem with respect to the interchange $n \to N+1-n$, which corresponds to a reflection in the plane passing through the middle of the cylinder. The solution a) is symmetric under such an interchange; the solution b), antisymmetric; and two nonsymmetric solutions of the type c) transform into each other under such an interchange.

If $\gamma_1 < 0$, $|\gamma_1| < \gamma_3$, and $\gamma_2 > 0$, then a solution of the type a) is realized. At large C, (3.5) approaches its asymptotic form even more rapidly; for example $\delta A_{n+1}/\delta A_n = 0.17$ for $C = 1$.

For $C \geqslant \frac{1}{2}$, we can, by assuming $A_2 = A^0$, easily find the flexure amplitudes in the extreme pairs directly from the Eqs. (3.4):

$$|A_1|^2 = |A_N|^2 = |A^0|^2[1-1/2(2C+1)]. \tag{3.20}$$

It can, for example, be seen that even with $C = \frac{1}{2}$, $|A_1|^2$ differs little from $|A_0|^2 = \gamma/\eta$: $|A_1|^2 = 0.75|A^0|^2$.

Summarizing the results of Subsecs. 2 and 3 of this section, we can say that, when $a\eta > bT$, the steady-state solution to Eqs. (3.5) with null "boundary conditions" is stable for any supercriticality. For small γ/a the profile of $|A_n|$ has, in accordance with (3.16), the shape of a half-wave; with increasing γ, the profile of $|A_n|$ becomes flatter, approaching, in accordance with (3.19) and (3.20), $(\gamma/\eta)^{1/2}$. If, on the other hand, $a\eta < bT$, then the steady-state solution to Eqs. (3.4) is stable only at small supercriticalities, when the profile of $|A_n|$ has, in accordance with (3.16), the shape of a half-wave. Numerical experiments, which we describe in the following section, show that at $a\eta < bT$ the steady-state solution to Eqs. (3.4) loses its stability with increasing γ, a sequence of bifurcations, which separate the various regimes of the temporal behavior of $A_n(t)$, being observed.

We may think that the "stable" case $a\eta > bT$ is realized in experiments[13] with a narrow clearance, as well as in experiments with a wide clearance for the $m=1$ flexural mode in a flow with $N=14$, experiments which are characterized by the fact that $|A_n|^2 = \mathrm{const}$ in a broad range of Reynolds numbers (see Table I). On the other hand, the complex dynamics of $I_6(t)$ decribed in the second section should be due to the instability of the solutions to (3.4) that arises when $a\eta < bT$. The stochastization of the flow in the case in which $a\eta > bT$ should proceed along another path, namely, via the excitation of new fast motions. Apparently, we can describe certain features of this phenomenon if we restrict ourselves to the processes occurring in one vortex pair. Yahata[8] recently simulated these processes with the aid of a Galerkin expansion of the Navier–Stokes equations, in which 32 selected functions were retained. A good agreement is obtained with experiments[13] on the critical number for the transition to the stochastic regime, but

the broad-band component, B, arises at an entirely different place in the spectrum.

§4. THE COMPLEX BEHAVIOR OF A SYSTEM OF INTERACTING TAYLOR VORTICES. A NUMERICAL EXPERIMENT

1. The procedure for the numerical experiment

Let us choose as dimensionless time $\bar{t}$ and dimensionless amplitude $\bar{A}$ the following quantities:

$$\bar{t}=at, \quad \bar{A}=A(\eta/\gamma)^{\frac{1}{2}}. \tag{4.1}$$

Then Eqs. (3.4) assume the form

$$\frac{d\bar{A}_n}{d\bar{t}}=\Gamma[1+(i\Theta-1)|\bar{A}_n|^2]\bar{A}_n+\frac{1}{4}(1+iB)(\bar{A}_{n+1}+\bar{A}_{n-1}-2\bar{A}_n),$$

$$\Gamma=\gamma/a, \quad \Theta=T/\eta, \quad B=b/a. \tag{4.2}$$

We shall, in investigating them, restrict ourselves to the $N=15$ case, which corresponds to the experimental situation, and use the null "boundary conditions"

$$\bar{A}_0=\bar{A}_{16}=0. \tag{4.3}$$

The numerical modeling of the problem (4.2),(4.3) reduces to the study of the trajectories $\bar{A}_n(\bar{t})$ over periods of time much longer than the characteristic periods of the motion. Therefore, the numerical solution requires the use of stable difference schemes that do not lead to the buildup of computational errors over the long time intervals. We used the Runge–Kutta fourth-order process. It guarantees the attainment of a steady-state solution and the constancy of this solution to within 10^{-5} over arbitrarily long periods of the time $\bar{t}$. In the regime of periodic auto-oscillations, their amplitude $\delta\bar{A}$ and period τ did not depend on the choice of the step $\Delta\bar{t}$ to within 10^{-5} when $\Delta\bar{t}<0.2\tau$. In the numerical simulation of the stochastic auto-oscillations at high supercriticalities, we encountered additional difficulties connected with the rapid divergence of the trajectories $\bar{A}_n(\bar{t})$ that are close in their initial values. For example, for $\Theta=10$, $\Gamma=0.144$, and $B=1.25$, two trajectories starting with one and the same initial condition, and differing in the steps chosen for their computation ($\Delta\bar{t}=0.15$ and $\Delta\bar{t}=0.3$, which are respectively 0.008 and 0.016 of the characteristic period, $\tau\approx19$, of the motion), completely diverged (by a value of the order of the attractor dimension) over a period of time $\bar{t}\approx80$. In this case a one-percent loss in accuracy due to the error made in the difference approximation with $\Delta\bar{t}=0.15$ was reached roughly by $\bar{t}\approx60$. All this, generally speaking, makes it impossible to study the details of the behavior of the system over time intervals longer than the "confidence interval." But this circumstance is of no importance in the study of the statistics of the process, since the dynamical stochasticity due to the hyperbolicity of the system is stronger than the stochasticity arising on account of the approximation errors.[3] The numerical experiments agree with this in the cases in which the values chosen for the coefficients of the system (4.2) are not too close to the bifurcation values. Thus, for example, the power spectra computed with $\Delta\bar{t}=0.15$ and $\Delta\bar{t}=0.3$ for $\Theta=10$, $\Gamma=0.2$, and $B=1.25$ coincide within the limits of the confidence interval stipulated by the finiteness of the observation time.
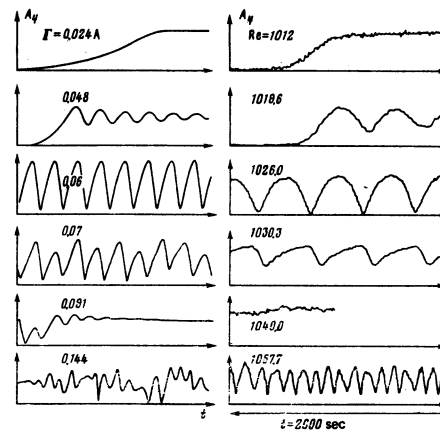

FIG. 5. Time dependences of the intensity of the ω_6 motion in the fourth vortex pair after an abrupt change in the Reynolds number. On the right are the results of the natural experiment; on the left, the results of the numerical experiment with $\theta=10$, $B=1.25$, and $\Gamma=0.56(\text{Re}-\text{Re}_1)/\text{Re}_1$.

2. The dynamical properties of the trajectories

The preliminary numerical experiments involved the visual observation of the trajectories $|A_n(t)|$ for very different values of the coefficients, Γ, Θ, and B, of the Eqs. (4.2). Characteristic time dependences of $|A_4(t)|$ are shown on the left hand side of Fig. 5. It can be seen that the amplitude $|A_4(t)|$ can approach a limiting value aperiodically ($\Gamma=0.024$) or with damped oscillations (Γ is equal to 0.048 or 0.091), appear as a periodic function of the time, or behave in a chaotic fashion. We can get a clearer idea about the behavior of the system by considering the projection of the phase trajectory on certain planes. In time, the phase trajectory of the system (4.2) gets, irrespective of the initial values of the phases, drawn to attractors of one or another degree of complexity: to a fixed point, to a limit cycle, or to more complex attractors. Examples of some of them are shown in Fig. 6. We cannot at
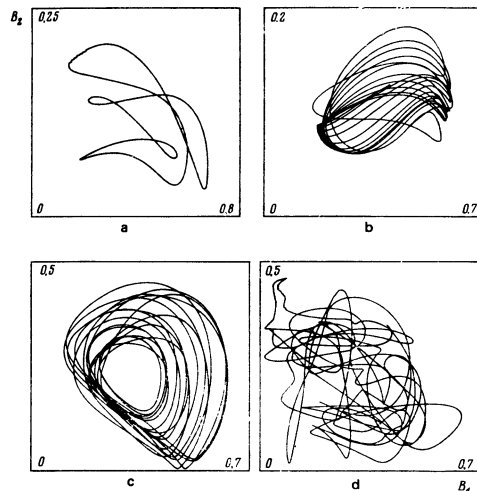

FIG. 6. Examples of the projections of the phase trajectories of Eqs. (4.2) on suitable planes: a) a triple limit cycle; b), c), and d) stochastic attractors of various degrees of complexity.
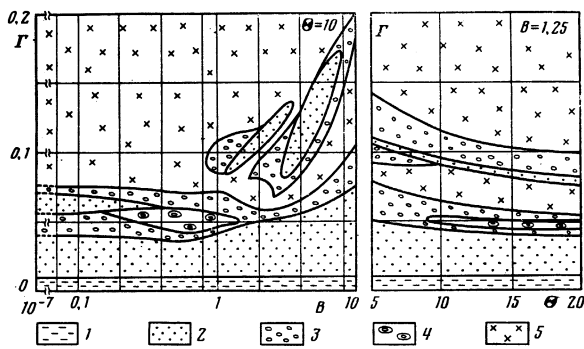
FIG. 7. Regions of different types of behavior of the system of equations (4.2): 1) and 2) equilibrium configurations, 3) limit cycles, 4) two-dimensional tori, and 5) complex attractors.

this stage of the investigations distinguish a complex limit cycle or a long transitional regime from really stochastic behavior. It is easy to record only relatively simple limit cycles or equilibrium configurations The results obtained at this level of rigor are indicated in Fig. 7, where the regions of different types of behavior of the system are marked out in the (Γ, B) plane for $\Theta = 10$. The ordinates are the values of the ratio $\Gamma = \gamma/a$, which is proportional to the Reynolds number. By choosing ratios of B and Θ, we can obtain in a numerical experiment the same sequence of bifurcations (as Re is increased) as is obtained in experiment. For example, for the arbitrarily chosen value $\Theta = 10$, such an agreement is observed at $B = 1.20-1.30$. Indeed, as Re is increased in a natural experiment (see Fig. 3), and as Γ is increased in a numerical experiment (see Fig. 5), a stable limit point is replaced by a limit cycle with sinusoidal modulation, then the stable point reappears,nonly to be replaced by a stochastic attractor. If we set $\Gamma = 0.56(\mathrm{Re} - \mathrm{Re}_1)/\mathrm{Re}_1$ here, then the measured and computed bifurcation Reynolds numbers are in qualitative agreement.

Also resembling each other are the experimental and temporal $|A(t)|$ dependences corresponding to the stepwise variation of the Reynolds number (see Fig. 5).

TABLE II. Level of excitation of the system in the numerical experiment with different Γ and $\theta = 10$.

Γ	n									
	1	2	3	4	5	6	7	8	9	10
0.08	100	26	28	2.2	6.7	0.2	2.2	0.0	0.9	0.0
	111	27	26	2.1	2.0	0.2	0.2	0.0	0.0	0.0
0.15	100	61	56	17	20	2.8	5.7	0.8	2.0	0.3
	106	61	60	17	16	2.4	2.1	0.7	0.5	0.3
0.20	21	100	73	4.1	10	3.6	5.5	0.6	1.6	0.3
	8.5	102	99	4.1	1.8	4.4	2.4	0.5	0.3	0.2
0.06	100	34	34	10	13	1.5	3.5	0.5	1.3	0.1
	109	34	32	11	10	1.3	1.0	0.4	0.2	0.1
0.08	100	36	35	12	15	3.0	4.9	0.9	1.8	0.3
	109	36	33	12	12	2.9	2.5	0.8	0.5	0.3
0.15	100	56	53	32	30	12	12	4.5	5.2	1.9
	104	65	60	32	30	12	10	4.5	3.5	1.9
0.20	100	87	73	45	39	21	20	9.9	9.5	4.5
	101	86	77	45	39	21	18	9.9	7.8	4.5

Note. The upper part of the Table (for $\Gamma = 0.08$; 0.15; 0.20) pertains to the case $B = 10$; the lower part, to the case $B = 1.25$. The first line for each Γ gives (in percent) the ratio of the intensity $I_n = \langle |B_n|^2 \rangle$ to the intensity of the most strongly excited harmonic. The second line gives the eigenvalues of the matrix $100 \langle B_n B_m^* \rangle / \max I_n$.

But at this stage it is too early to speak of complete agreement between the real and numerical experiments. In particular, in the real experiment we observed (see Fig. 3) a limit cycle after a stochastic attractor, which was not found in the numerical experiment. It is possible that this discrepancy is due to the fact that the relation $\Theta = 10$ is an arbitrarily chosen one. Generally speaking, we should carry out special experiments to independently measure the coefficients in the phenomenological model (4.1)–(4.3). Nevertheless, it is even now quite safe to say that this model indeed describes the initial phase of the turbulization of the Couette-Taylor flow. Therefore, a more detailed study of the statistical properties of the attractor in this model is of definite interest. The first results of such an investigation are presented in the following section.

§5. THE STATISTICAL PROPERTIES OF THE TRAJECTORIES IN THE PHENOMENOLOGICAL MODEL

1. The upper limit of the attractor dimensionality

The phase space of the system of the fifteen complex Eqs. (4.2),(4.3) has a dimensionality of 30. But a much smaller number of degrees of freedom should be excited when $\Gamma \ll 1$. This can easily be verified by considering the representation (3.12) of the harmonics diagonalizing the linear part of the equations. Indeed, for $\gamma \ll a$ only the harmonics with small n fall in the instability region. For example, at $\Gamma = 0.05$ only the first two harmonics are unstable; at $\Gamma = 0.1$, the first three; and at $\Gamma = 0.2$ only for the first four of the fifteen harmonics is $\gamma_n < 0$. It is precisely the unstable harmonics that should be most effectively excited. They are the driving force for all the rest. The greatest response should come from the low-n harmonics, which have the least margin of stability; the harmonics with large n should be effectively suppressed.

On the whole, experiment corroborates these extremely simplified arguments (Table II). It can be seen that, with the exception of one case, the most intense is the first harmonic; the intensity of excitation decreases monotonically with increasing harmonic number in a system of even and odd harmonics. If we assume that the weakly excited harmonics (e.g., with relative intensities of less than 5% of the highest intensity) virtually do not affect the dynamics of the system, then, for $\gamma \ll a$, the requisite number of differential

TABLE III. Number of harmonics whose levels of excitation are more than 5% of the maximum level (for $\theta = 10$ and different Γ and B).

B	Γ			
	0.06	0.08	0.15	0.20
10	–	4(3)	6(5)	5(3)
1.25	5(5)	5(5)	8(7)	9(9)

Footnote. Indicated in the brackets is the number of eigenvalues of the correlation matrix $\langle B_n B_m^* \rangle$ that have magnitudes of more than 5% of the maximum eigenvalue.

569   Sov. Phys. JETP 53(3), March 1981

L'vov et al.   569

TABLE IV. The normalized correlation matrices $\langle B_n B_m^* \rangle$ for $B = 1.25$, $\theta = 10$, $\Gamma = 0.08$ (upper part) and $B = 1.25$, $\theta = 10$, $\Gamma = 0.2$ (lower part).

n	m									
	1	2	3	4	5	6	7	8	9	10
1	100	3.3	32	-0.4	32	-0.7	38	-0.6	44	-0.7
2	0.3	34	1.5	-5.5	0.3	-7.6	0.8	-10	0.5	-11
3	-0.4	0.1	34	1.0	40	-1.3	52	-1.5	59	-0.6
4	0.4	-0.3	0.0	12	1.4	-14	-1.4	-20	-0.1	-19
5	-0.4	-0.2	-1.8	-1.8	15	0.0	55	-2.5	65	-1.0
6	0.8	1.9	0.4	22	2.2	3.0	1.3	-12	-1.1	-5.7
7	0.0	0.6	4.2	0.7	-15	-3.9	4.9	0.7	70	-1.0
8	0.7	3.9	-2.2	-11	-2.2	9.7	0.0	0.9	0.3	12
9	0.7	-0.6	-1.7	1.7	-7.6	-1.1	1.8	1.4	1.7	0.4
10	1.2	-4.6	0.6	-6.8	-1.1	10	1.2	0.4	0.3	0.3
1	100	1.2	1.1	0.3	4.6	-0.1	5.1	0.0	5.8	0.3
2	0.4	87	1.0	-0.8	0.0	-0.9	-0.4	-2.1	0.6	-0.1
3	0.1	-0.6	73	0.6	16	0.3	17.4	1.2	20	0.3
4	0.5	-0.3	1.0	45	0.2	-4.5	-0.4	-1.7	-1.1	-1.9
5	0.0	-0.7	-0.4	0.6	39	0.2	26	0.7	27	0.0
6	0.1	-1.6	0.7	-3.0	-0.7	21	0.4	-2.7	-1.0	-2.1
7	0.0	-0.6	-3.0	0.8	2.1	1.1	20	1.2	28	0.0
8	0.7	-8.8	2.2	2.5	-0.8	0.2	-3.0	9.9	0.5	-0.6
9	-4.7	1.9	7.8	0.4	4.8	2.6	3.2	6.2	9.5	0.3
10	4.3	4.7	0.2	-1.8	-1.8	-0.9	-4.5	-1.0	-4.5	4.5

Footnote. The diagonal elements are given by the ratio $100 \langle |B_n|^2 \rangle / \max \langle |B_n|^2 \rangle$; the off-diagonal elements determine the correlation coefficient $K_{nm} = \langle B_n B_m^* \rangle (\langle |B_n|^2 \rangle \langle |B_m|^2 \rangle)^{-1/2}$. The numbers above the principal diagonal are values of the real part of K_{nm} multiplied by 100, while those below it are values of $100 \, \text{Im}\{K_{nm}\}$.

equations reduces from fifteen to the number indicated in Table III. In geometric terms, we can say that the attractor of the dynamical system in question is oriented in phase space almost perpendicularly to the coordinate axes corresponding to the high-n harmonics. But the harmonic representation (3.12) is not the best linear unitary change of variables (i.e., choice of orientation of the coordinate axes of phase space) for which the number of intensely excited variables is a minimum. To find these variables

$$C_n = V_{nm} A_m = U_{nm} B_m,$$
$$VV^{-1} = 1, \quad UU^{-1} = 1, \tag{5.1}$$

we must compute the single-time correlation matrix $\langle A_n A_m^* \rangle$, and find the unitary matrix, V_{nm}, that reduces it to the diagonal form. This procedure is equivalent to the approximation of an attractor by a multidimensional ellipsoid and the determination of the orientation and magnitudes of the principal axes $\langle |C_n|^2 \rangle^{1/2}$. The intensities $\langle |C_n|^2 \rangle$ are the eigenvalues of the correlation matrices $\langle A_n A_m^* \rangle$ or $\langle B_n B_m^* \rangle$. In Table IV we give the correlation matrices $\langle B_n B_m^* \rangle$ as computed for $\Theta = 10$, $B = 1.25$, and the two values $\Gamma = 0.08$ and 0.2. It can be seen that the odd harmonics are quite strongly correlated, the correlation factor K_{nm} being almost real, and increasing with increasing n and m. The even harmonics are more weakly correlated among themselves than the odd ones. The motions of the even and odd harmonics are virtually not correlated. As the supercriticality (i.e., the ratio $\Gamma = \gamma/a$) increases, the degree of correlation in the motions of the harmonics decreases. All these factors (with the exception of the reality of K_{nm} for the odd harmonics) can be explained on the basis of the structure of the equations (3.12), (3.13), for the harmonics.

The eigenvalues, $\langle |C_n|^2 \rangle$, of the correlation matrix are given for some values of the parameters in Table
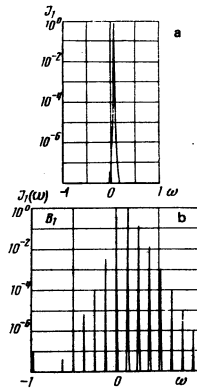

FIG. 8. Power spectra corresponding to: a) an equilibrium configuration and b) a limit cycle; $\theta = 10$, $B = 1.25$, and $\Gamma = 0.04$; 0.06.

II, while Table III gives the number of the eigenvalues $\langle |C_n|^2 \rangle$ whose magnitudes exceed 5% of the maximum eigenvalue. It can be seen that the transition to the "best orientation of the coordinate axes," C_n, allows a further reduction of the required number of differential equations in comparison with the number required in the case of the harmonic representation.

Thus, we have obtained the upper limit for the dimensionality of the attractors as a function of the parameters of the problem, including the supercriticality Γ. Naturally, this estimate is too high in certain cases. For example, for $\Theta = 10$, $B = 1.25$, and $\Gamma = 0.06$, the attractor is a limit cycle, i.e., the dimensionality is equal to one, and, with an appropriate choice of variables, the behavior of the system can be described by one differential equation. But the variables C_n have the advantage that they can easily be explicitly indicated in (5.1) with the aid of the unitary matrix U that diagonalizes the correlation matrix $\langle B_n B_m^* \rangle$.

2. The power spectrum

In the preceding subsection we considered the single-time correlation matrix $\langle B_n(t) B_m^*(t) \rangle$. Here we discuss the results of a numerical experiment involving its diagonal elements in the case of noncoincident times: $J_n(\tau) = \langle B_n(t) B_n^*(t + \tau) \rangle$. Instead of the quantity $J_n(\tau)$, it is convenient to use its Fourier transform, i.e., the power spectrum of the harmonics:

$$J_m(\omega) = \langle |B_m(\omega)|^2 \rangle, \tag{5.2}$$

where $B_m(\omega)$ is the Fourier transform of $B_m(t)$, while
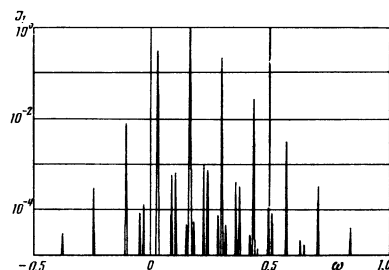

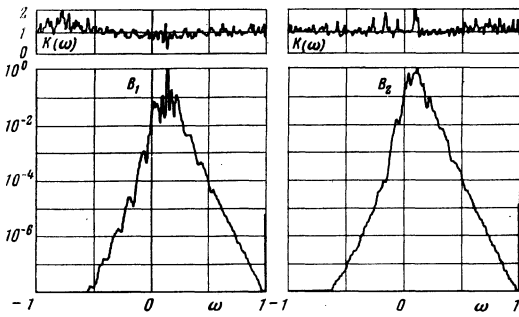FIG. 9. Power spectra corresponding to a double limit cycle ($\Gamma = 0.066$).

FIG. 10. Power spectra and excesses of the first and second harmonics in the region of stochastic behavior ($\Gamma = 0.08$).

⟨. . .⟩ denotes, as in (2.1), averaging over the successive $B_m(t)$-realization segments.

The spectrum a) (see Fig. 8) corresponds to a simple limit cycle with a trivial time dependence: $B_m(t) \propto \exp(-\Omega t)$ [the finite width of the line is explained by some imperfection in the computational algorithm for (5.2)]. In a coordinate system rotating with frequency Ω, this situation corresponds to an equilibrium configuration; the regions 2) with this behavior have been marked out in the parameter plane (see Fig. 7). The spectrum b) in Fig. 8 was computed in the region 3) of the parameter plane, i.e., in the region of limit cycles (in a rotating reference system). It is noteworthy that the intensities of the satellites decrease exponentially with increasing distance from the central Ω line. In Fig. 9 we show the spectrum corresponding to a double limit cycle. We can see the splitting of the lines, which arises as a result of the noncoincidence of the periods of the first and second revolutions in the limit cycle.

The spectra shown in Figs. 10–12 were computed in the region 5) (complex attractors) of the parameter plane, where the trajectory of the system appears to be stochastic. We used sufficiently representative $B_n(t)$-realization segments containing up to ten γ^{-1} characteristic times. In this case the spectra computed with essentially different initial conditions coincide within the limits of the confidence interval, which indicates the stochasticity (the "nonremembrance" of the initial conditions) and the stationarity of the system's trajectory.

The spectra of the harmonics shown in Figs. 10 and 11 were computed in the region of stochastic behavior with the same $\Theta = 10$ and $B = 1.25$ and different supercriticalities $\Gamma = 0.08$ (see Fig. 10) and $\Gamma = 0.2$ (see
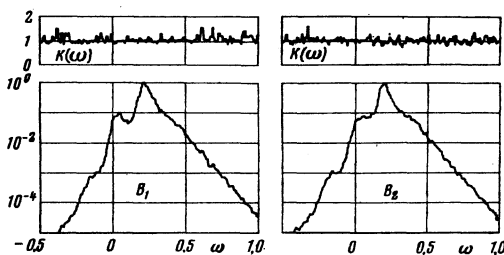

FIG. 11. Power spectra and excesses of the first and second harmonics in the region of stochastic behavior ($\Gamma = 0.2$).
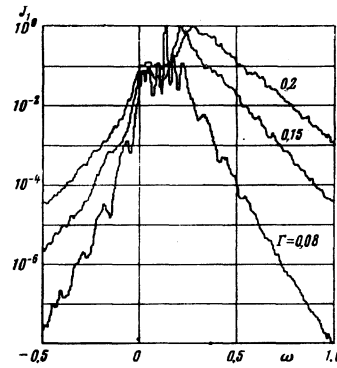

FIG. 12. Comparison of the power spectra of the first harmonic for three values of $\Gamma = 0.08$; 0.15; 0.2.

Fig. 11). Also shown in these figures are plots of the "excess" $K(\omega)$, computed from the formula

$$K(\omega) = [\langle |B_m(\omega)|^4\rangle / J_m^2(\omega)] - 1.$$

We shall discuss the quantities $K(\omega)$ below; here we consider only the evolution of the spectra $J_m(\omega)$ with increasing supercriticality (at fixed $\Theta = 10$ and $B = 1.25$).

The value $\Gamma = 0.08$ lies quite close to the region of dynamical behavior: the trajectories are periodic when $\Gamma = 0.06$ and $\Gamma = 0.1$. Therefore, when $\Gamma = 0.08$, the attractor should contain slightly unstable cycles, near which a trajectory can exist for quite a long time. Accordingly, the power spectrum of the odd harmonics with small $n(=1; 3; 5)$, on which the cycle is probably concentrated, contains strongly pronounced peaks. It is noteworthy that the asymptotic form of the spectra in the region far from the line center is, to a high degree of accuracy, exponential (a straight line in the logarithmic scale):

$$J_m(\omega) \propto \exp(-|\omega - \Omega| / \Delta_\pm), \qquad (5.3)$$

the indices $\Delta_\pm$ of the exponential functions for the right and left slopes being practically independent of the harmonic number.

At high supercriticalities we move away from the stability region of the limit cycles, which then cease to appear in the spectrum (see Fig. 11). It is characteristic that the spectra of all the harmonics are very similar and are even better described by the exponential function (5.3). The indices for the exponential function increase with increasing supercriticality (see Table V and Fig. 12).

In conclusion of this section, let us note that the excess $K(\omega)$ computed in the region of stochastic behavior (see Figs. 10 and 11) differs little from unity. This in-

TABLE V. Index $\Delta_\pm$ of the exponential function determing $J_m(\omega)$ according to the formula (5.3) for $\theta = 10$, $B = 1.25$, and different Γ.

Γ	$\Delta_{+/a}$	$\Delta_{-/a}$	$\Delta_{+/\gamma}$	$\Delta_{-/\gamma}$
0.08	0.051	0.045	0.64	0.57
0.15	0.079	0.063	0.53	0.42
0.20	0.11	0.079	0.54	0.39

dicates that the statistics of the random processes $B_n(t)$ is in a sense nearly Gaussian, and we may hope that an analytical statistical description of a system of interacting Taylor vortices that uses this fact will be successful.

CONCLUSION

In this paper we have demonstrated the possibility of describing the initial phase of turbulence with the aid of a finite-dimensional dynamical model in the particular case of circular Couette flow. The complex attractor in the phase space of this model is the image of the turbulent motion of the liquid. Formally, the phenomenological model proposed by us can be derived from the Navier–Stokes equations in much the same way as the Landau equation is derived, but in this case allowance is made for the degeneracy of the bifurcating solution. It would have been useful to try with the aid of a computer to calculate the coefficients in the phenomenological equations (3.4) and find the region of their applicability and the structure and magnitudes of the correction terms. It is necessary to carry out measurements to verify the assumptions underlying this model: for example, the hypothesis that $A(r,t) = A(t)f(r)$. It is also necessary to investigate the spatial profile of the azimuthal modes along the whole cylinder and the mutual correlation of the motions in the various vortices, and to carry out a much more detailed comparison of the results of the natural and numerical experiments [within the framework of Eqs. (3.4)]. After this, it will make much more sense to carry out a detailed investigation of the structure of the complex attractor in the phase space of Eqs. (3.4): the study of the character of the trajectory dispersal, the functions of the Poincaré sequence, etc. Of special interest are the problems pertaining to the transition from the dynamical description of the system within the framework of (3.4) to a statistical description by methods worked out in the theory of turbulence. The following questions arise: How close to Gaussian is the statistics of the $A_n(t)$ motions? On what does the degree of this closeness depend, and in which region of the parameters of the model is Kraichnan's direct-interaction approximation applicable? How good is, and what range of phenomena can be described within the framework of, this approximation? Many of the above questions are interesting in themselves, but, as links of a single chain connecting the general Navier–Stokes equations with turbulent motion in a specific flow, they are fundamental questions.

It gives the authors much pleasure to express their gratitude to Yu. E. Nesterikhin for constant support and attention, F. A. Zhuravel' for his selfless labor in writing the program for the data collection and display system. We are also grateful to Z. B. Kruglyak and E. N. Utkin for the experimental equipment and for their help in the performance of the experiments. We thank E. A. Kuznetsov and M. D. Spektor for stimulating and useful discussions.

APPENDIX

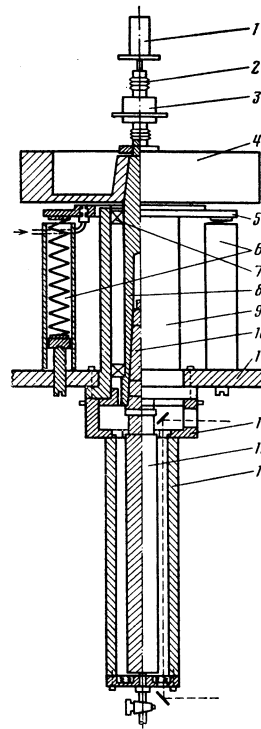We used the experimental setup whose mechanical construction is shown in Fig. 13. The principal unit is

FIG. 13. Hydrodynamic stand.

a spindle 8), which rotates in precision ball bearings 7) secured in a race on a bedplate 11). At the top of the spindle is a massive (40 kg) flywheel 4), and to the bottom is attached via a Morse cone 10) a stainless steel inner cylinder 13) of diameter 35 mm. The whole rotating part of the apparatus is borne on an air-lubricated bearing 5). The spring suspension 6) is adjusted in such a way as to relieve the bearing 7) of the vertical stress and minimize the frictional noise. The flywheel is set in rotation by an electric motor 1) via bellows 2). The angular velocity is controlled by an electronic circuit whose follow-up instrument is a precision tachometer 3). The technical measures taken allow us to to maintain the period of rotation T to within 10^{-4} T or less (in the range of T from 20 to 0.1 sec), and guarantee less-than-5-μm wobble of the base of the inner cylinder (for a gap of 1 cm). The outer cylinder 14) in the above-described experiments was made of stainless steel, and had an internal diameter of 55 mm. Its mounting 12) allows us to make the setting coaxial with the inner cylinder to within 5 μm. The upper and lower ends of the cylinder are made of optical glass. The laser beams are distributed along the azimuth of the cylinders, and reach the experimental volume from above in accordance with Fig. 13. The whole setup is placed in a box with thermal insulation, which also contains a thermostat that maintains the air temperature to within ± 0.02 °C. The temperature of the outer cylinder was measured with a 2801a Hewlett–Packard quartz thermometer.

[1] Let us note in this connection that Fenstermacher et al.[13] have also observed in an experimental investigation of the laminar–turbulent flow transition in a Couette flow with a narrower gap a narrow spectral line, which they interpret as a purely periodic regime. But a slow modulation is dis-

572   Sov. Phys. JETP 53(3), March 1981

L'vov et al.   572

tinctly visible in the realization range shown in Fig. 5a of their paper.[13]

[1]D. Ruelle and F. Takens, Commun. Math. Phys. 20, 167 (1971).

[2]M. I. Rabinovich, Usp. Fiz. Nauk 125, 123 (1978) [Sov. Phys. Usp. 21, 443 (1978)].

[3]Ya. G. Sinaĭ, in: Nelineĭnye volny (Nonlinear Waves), Nauka, Moscow, 1979, pp. 192–212.

[4]H. F. Greveling, J. F. de Paz, J. Y. Baladi, and R. J. Schoenhals, J. Fluid Mech. 67, 65 (1975).

[5]E. N. Lorenz, J. Atmos. Sci. 20, 130 (1963).

[6]D. V. Lyubimov, G. F. Putin, and V. I. Chernatynskiĭ, Dokl. Akad. Nauk SSSR 235, 554 (1977) [Sov. Phys. Dokl. 22, 360 (1977)].

[7]J. B. McLaughlin and P. C. Martin, Phys. Rev. A 12, 186 (1975).

[8]H. Yahata, Prog. Theor. Phys. 61, 791 (1979).

[9]E. A. Kuznetsov, V. S. L'vov, Yu. E. Nesterikhin, et al., Preprint, Inst. Autom. and Electrometry, Novosibirsk, No. 58 (1977).

[10]T. B. Benjamin, Proc. R. Soc. A 359, 1 (1978).

[11]V. S. L'vov and A. A. Predtechensky, Preprint, Inst. Autom. and Electrometry, Novosibirsk, No. 111 (1979).

[12]F. A. Zhuravel', Z. B. Kruglyak, E. A. Kuznetsov, V. S. L'vov, Yu. E. Nesterikhin, A. A. Predtechenskiĭ, V. S. Sobolev, and E. N. Utkin, Preprint, Inst. Avtomat. Élektrom., Sibirsk. Otd. Akad. Nauk SSSR, Novosibirsk, No. 103 (1979).

[13]P. R. Fenstermacher, H. L. Swinney, and J. P. Gollub, J. Fluid Mech. 94, 103 (1979).

Translated by A. K. Agyei